Simulation of the AGILE gamma-ray imaging detector performance: part I

Francesco Longo[a,d], Veronica Cocco[b,d,*], Marco Tavani[c,b,d]

[a] *Università degli Studi di Ferrara and INFN Sezione di Ferrara, Italy*
[b] *Università degli Studi ''Tor Vergata'' and INFN Sezione di Roma II, Italy*
[c] *Istituto di Fisica Cosmica, CNR, Milano, Italy*
[d] *Consorzio Interuniversitario Fisica Spaziale, Torino, Italy*

Abstract

We present in this paper the results of a comprehensive GEANT simulation of the Gamma-Ray Imaging Detector (GRID) being developed for the AGILE space astrophysics mission. The GRID is designed to be sensitive in the ~ 30 MeV–50 GeV energy range, with excellent imaging and timing capabilities, and with a very large field-of-view (~ 3 sr). In this paper (Paper I) we present the GRID baseline geometry, a model for the charged particle and albedo-photon backgrounds for an equatorial orbit of 550–600 km altitude, and the main results of the first level (Level-1 Trigger) on-board data processing. Our simulations show that the GRID Level-1 data processing is expected to be capable of decreasing by a factor of ~ 20 the charged particle background (from ~ 2 kHz to below 100 Hz), and by a factor of ~ 30 the albedo-photon background. The gamma-ray photon detection efficiency by the imaging GRID is simulated to be particularly efficient, varying between 39% and 17% depending on photon energies and incident directions. © 2001 Elsevier Science B.V. All rights reserved.

1. Introduction

AGILE is an Italian Space Agency (ASI) Small Scientific Mission dedicated to high-energy astrophysics [1,2]. The AGILE instrument is designed to detect and image photons in the ~ 30 MeV–50 GeV and 10–40 keV energy bands, with excellent spatial resolution and timing capability, and a very large field of view covering $\sim \frac{1}{5}$ of the entire sky at energies above 30 MeV [3]. Primary scientific goals include the study of AGNs, gamma-ray bursts, Galactic sources, unidentified gamma-ray sources, diffuse Galactic and extragalactic gamma-ray emission, high-precision timing studies and Quantum Gravity testing [3].

The AGILE Gamma-Ray Imaging Detector (GRID) consists of a Silicon-Tungsten Tracker, a

*Corresponding author. Dip. di Fisica, Universita di Roma ''Tor Vergata'', Via della Ricerca Scientifica 1, 00133 Roma, Italy. Tel.: +39-6-7259-4718; fax: +39-6-7259-4647.

E-mail address: veronica.cocco@roma2.infn.it (V. Cocco).

Cesium Iodide Mini-Calorimeter (MC), an Anti-coincidence system (AC) made of segmented plastic scintillators, and a Data Handling system (DH). The GRID is sensitive in the energy range ~ 30 MeV–50 GeV, and is designed to achieve an optimal angular resolution (source location accuracy ~ 5–$20'$ for intense sources), a very large field-of-view (~ 3 sr), and a sensitivity comparable to that of EGRET for on-axis (and substantially better for off-axis) point sources. The optimal performance of the AGILE GRID requires an efficient on-board selection of events aimed at maximizing the background rejection and the transmission of cosmic photon events. This task is carried out by the Data Handling (DH) System.

In the current (Paper I) and companion [4] papers we present the main results concerning the simulation of GRID events induced by the particle/albedo-photon background and by the cosmic gamma-rays. We study in detail different levels of the GRID on-board trigger and data processing. For the Monte Carlo simulations we used the numerical code GEANT (version 3.21) [5] and related subroutines. Our numerical results are in very good agreement with CERN beam-test results obtained by our group with electrons and photons in the 0.1–1 GeV energy range [6–8].

2. Cosmic gamma-ray signal and expected particle and albedo-photon background

2.1. Cosmic gamma-ray flux

The cosmic photon flux on the AGILE-GRID detector will be dominated by the diffuse gamma-ray emission, typically larger near the Galactic plane by a factor of 10 with respect to the high-Galactic-latitude. This latter emission has a flux of $\Phi \simeq 10^{-5}$ ph cm^{-2} s^{-1} sr^{-1} for photons above 100 MeV. Expected gamma-ray event rates for the AGILE-GRID depend on the pointed fields and can be given in the ranges (dominated by the diffuse gamma-ray emission): 0.02–0.1 ph s^{-1} for energies larger than 100 MeV and 0.1–1 ph s^{-1} for energies between 10 and 100 MeV. The contribution of point-like gamma-ray sources adds to these rates without changing their order of magnitude.

In the simulations we considered 4 classes of cosmic gamma-ray photons, divided in low-energy photons (25–50 MeV) and high-energy photons (400–1000 MeV); we used a power-law energy spectrum of index -2, and run simulations for two extreme cases: an input geometry of incidence angle between 0 and $10°$ off-axis, and an input geometry of incidence angle between 50 and $60°$ off-axis.

2.2. Charged particle background

An equatorial orbit near 550 km of altitude for the AGILE mission will provide a relatively low-background environment. The charged particle background for this orbit is known to be relatively stable, with an increase by a factor 10–100 near the South Atlantic Anomaly (typically influencing about 10% of the orbital duration). Taking into account data from SAS-2 [9,10] and Beppo-SAX [11] missions, out of the South Atlantic Anomaly we expect an average rate of charged particle background above ~ 1 MeV of ~ 0.3 particles cm^{-2} s^{-1} (mostly electrons/positrons with a $\sim 10\%$ contribution of protons).

In our simulations, based on spectral data from AMS [12–14] and MARYA [15], we considered the following background components: electrons (ELE), positrons (POS), primary high-energy protons (HE PROT) and secondary low-energy protons (LE PROT). We made the following assumptions: (1) we considered an "average equatorial position" and we assumed the AGILE z-axis pointed towards the sky for an unocculted GRID field of view; (2) we considered a spectrum averaged over the magnetic latitudes $|\lambda_{\mathrm{mag}}| = 0$–$11°$ for secondary protons, and $|\lambda_{\mathrm{mag}}| = 0$–$17°$ for electrons and positrons (values compatible with the AGILE equatorial orbit), regardless of longitude dependence; (3) we considered an isotropic distribution on a virtual sphere containing the satellite for particles below the geomagnetic cutoff (albedo leptons and secondary protons), and an isotropic distribution emitted from the upper hemisphere for the primary protons above the cutoff. The adopted particle spectra, which are fits of the AMS and MARYA data (calculated in [16]) are shown in Fig. 1. Their fluxes are normalized to
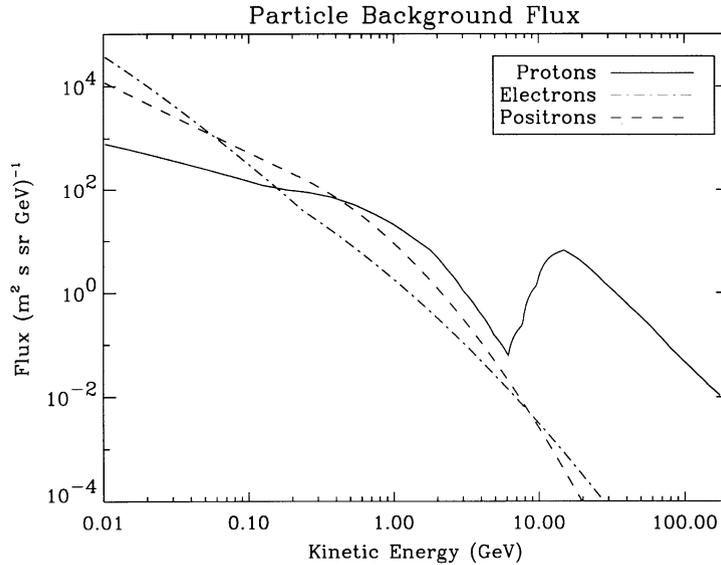
Fig. 1. Charged particle background for an equatorial orbit of 550 km (results from Ref. [16]) that we assumed in our calculations. Electron, positron and proton spectra were obtained by combined AMS-Shuttle Flight data and MARYA data. All particle components have an approximately isotropic distribution of incidence angles on the GRID, except the primary high-energy protons above the geomagnetic cutoff of ~ 6 GeV.

Table 1
Integrated particle flux rates

Particles	E_{min}	E_{max} (GeV)	$\mathscr{F}$ (cm^{-2} s^{-1} sr^{-1})	$\pi \mathscr{F}$ (cm^{-2} s^{-1})
Electrons	10 MeV	10	3.76×10^{-2}	0.1180
Positrons	10 MeV	10	2.67×10^{-2}	0.0840
Albedo protons	10 MeV	6	9.04×10^{-3}	0.0284
Primary protons	6 GeV	180	9.99×10^{-3}	0.0314

the values indicated in Table 1 and the total incidence rate on a surface is assumed to be ~ 0.3 particles cm^{-2} s^{-1} for particle kinetic energies above ~ 10 MeV.

2.3. Albedo gamma-ray background

The interaction of the charged cosmic-rays with the upper atmosphere induces a relatively strong and non-isotropic gamma-ray background. It peaks near the Earth horizon (corresponding to a zenith angle $\theta = 112°$ for an orbit of 550 km altitude), and has a characteristic East–West asymmetry (by a factor of ~ 4 in intensity near 40 MeV) [17].

In our simulations, we used a simplified but representative model of the albedo-photon emission, and we considered two geometries: (1) albedo-photons reaching the GRID "from below", a situation valid for the unocculted portions of the AGILE orbit (ALB-1 PHOT); (2) Earth covering half of the AGILE FOV, with a large fraction of albedo-photons reaching the GRID "from one lateral side" (ALB-2 PHOT). Based on balloon flight data [18–22] and SAS-2 data [17], we have assumed the following simplified spectrum

representing the average of the emission over the whole solid angle subtended by the Earth surface (~ 4 sr) at the height of 550 km:

$$\frac{\mathrm{d}N}{\mathrm{d}S\,\mathrm{d}t\,\mathrm{d}E\,\mathrm{d}\Omega} = \begin{cases} 0.08E^{-1.4} \text{ cm}^{-2} \text{ s}^{-1} \text{ sr}^{-1} \text{ MeV}^{-1} & \text{for } 1\text{ MeV} < E < 10\text{ MeV} \\ 0.5E^{-2.2} \text{ cm}^{-2} \text{ s}^{-1} \text{ sr}^{-1} \text{ MeV}^{-1} & \text{for } 10\text{ MeV} < E < 100\text{ GeV} \end{cases}$$

with a total flux $\mathscr{F} = 0.15$ cm^{-2} s^{-1} sr^{-1} in the energy range 1 MeV–100 GeV.

2.4. Background rejection

The ratio of charged particle events (penetrating the AC) to cosmic gamma-ray photon events is typically of order 10^3–10^4 for photons of energy 20–100 MeV, and 10^4–10^5 for photons above 100 MeV. Albedo-photons are larger than cosmic gamma-ray photons by factors between 10 and 100 (depending on the pointing geometry and energy range).

Clearly, is necessary to 'filter' the GRID events. This task is carried out by a hardware-implemented fast logic ("Level-1 trigger"), and by a set of asynchronous software algorithms and CPU processing ("Level-2 processing"). The adopted requirements for the DH processing depend on the downlink telemetry rate, assumed to be 512 kbit/s during the 10 min duration of satellite visibility from the ASI ground station in Malindi (Kenya). A main aim of the AGILE DH system is to provide an on-board filtering of events reducing the background rate to an acceptable value within a factor of 10–100 of the cosmic gamma-ray photon rate. A final filtering of the particle and albedo-photon background will be carried out on the ground by a dedicated software. The charged particle and the albedo-photon background models described in the previous sections were used in Monte Carlo simulations in order to optimize the DH processing.

3. The AGILE model and GRID detection assumptions

3.1. The AGILE model

A correct mathematical and physical model of the AGILE payload and spacecraft with all their relevant components is crucial to evaluate the GRID behaviour and performance. A general description of the AGILE instrument can be found in [1,3]. Simulation programs consider the following AGILE components (see Fig. 2): the spacecraft (bus) MITA and the AGILE payload, consisting of the CsI Mini-Calorimeter, the Silicon-Tungsten Tracker, the Anticoincidence system, the X-ray detector (Super-AGILE), the thermal shield, the mechanical structure and the lateral electronics boards. The AGILE components were modeled as follows:

(1) *MITA spacecraft*: The spacecraft (bus) MITA is represented by a box, made of carbon-fibers, containing 10 equidistant aluminum layers inserted in thin (100 μm) carbon-fiber structures; every aluminum layer is 1.1 cm thick for a total weight of 128 kg.
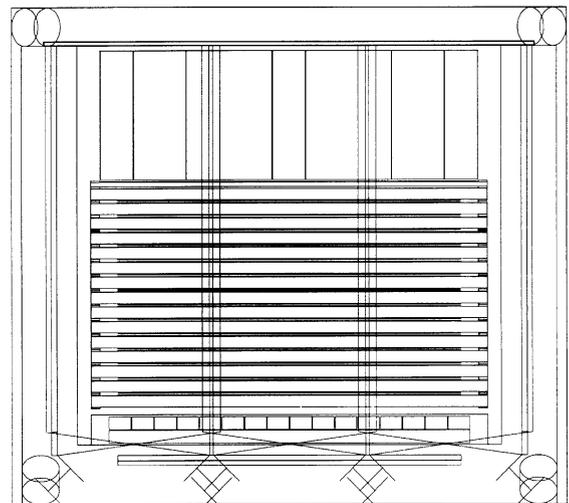

Fig. 2. AGILE payload: from the bottom the different volumes are: the DH box, the 2 planes of the Mini-Calorimeter, the 14 layers of the Silicon Tracker, Super-AGILE, the top AC panel. Also the lateral AC panels with the photomultipliers and the thermal shield are visible. The overall dimensions are: length of 62.55 cm, width of 62.55 cm and height of 54.02 cm. The GRID active volume dimensions are: $38.06 \times 38.06 \times 21.078$ cm^3 including the Tracker planes from the top sheet of the first tungsten layer to the bottom sheet of the last silicon-y plane.

(2) *Mini-Calorimeter*: The Mini-Calorimeter is modeled by two planes, each containing 16 CsI bars, oriented as the *y*-axis in the upper plane and as the *x*-axis in the lower plane. The CsI bars are 1.4 cm thick and have a pitch of 2.4 cm. They are inserted in a carbon-fiber structure 0.1 cm apart from each other. The distance between the *X* layer and the *Y* layer is assumed to be 0.1 cm. The Mini-Calorimeter is placed directly above the bus MITA, at a 0.5 cm distance from the Silicon Tracker.

(3) *Silicon Tracker*: The Silicon Tracker is made of 14 detection planes, with a distance between consecutive planes of 1.6 cm and a distance between the *X* and *Y* layers in each plane of 0.16 cm; the first 12 planes contain also a tungsten layer each (245 μm thick). Each silicon layer is composed of 16 tiles of 9.5×9.5 cm^2 each, with a pitch of 121 μm (each tile contains 768 strips) and a thickness of 410 μm. In our model there are also the honeycomb support, the aluminum inserts connecting the tracker planes with the main structure of the satellite, and the Front-End electronics chips (3 TA1 for each ladder). Every tracker plane is composed by a Carbon-fiber structure (500 μm thick) supporting an aluminum honeycomb. Under the carbon-fiber are glued the tungsten layer (for the first 12 planes), one layer of kapton (100 μm thick) with a copper coating (15 μm thick) and the *X* silicon layer. Under the *X* layer there are the *Y* layer and another kapton–copper layer, which in the reality are glued to the next plane structure. On the same structure are glued also the ceramic hybrids which sustain the TA1 silicon chips. The global structure is composed by 14 *X* and *Y* detectors layers and by 15 structure supports; the total tracker height is 24 cm.

(4) *Anticoincidence system*: The AC system is made of a top panel of plastic scintillator ($54 \times 54 \times 0.5$ cm^3) and 3 overlapping panels for each side of the AGILE Tracker (0.6 cm thick, 18.1 cm large and 44.4 cm high). The AC plastic panels are inserted in a carbon-fiber structure (500 μm thick) and are supported by some aluminum inserts; the trapezoidal form of the lateral panels is described in a proper way. We have inserted also a schematic description of

the photomultipliers and their casings. The AC system surrounds the Mini-Calorimeter, the Silicon Tracker and Super-AGILE, and is positioned above the bus MITA. Fig. 3 shows the adopted model.

(5) *X-ray detector* (*Super-AGILE*): The X-ray detector is made substantially by these elements: a silicon detection layer, a collimation system, a gold mask. A tungsten ring is positioned below the Si detection plane in order to reduce the diffuse photon background. The detection layer is divided in 16 tiles with the same characteristics of the tracker tiles, described in a realistic way, with the silicon microstrips and the Front-End electronics. We have modeled also the honeycomb and carbon-fiber support structure; the detectors and the support of the coded mask are glued on this structure. The silicon detector is placed over the tracker, while the distance between the silicon detector and the gold mask (90 μm thick) is fixed to be 14 cm. Also the collimation system, made of an ultra-light carbon-fiber structure (500 μm thick), is described in great detail (Fig. 4). Its internal panels are coated with a 75 μm thick gold layer, in order to reduce the contribution from the
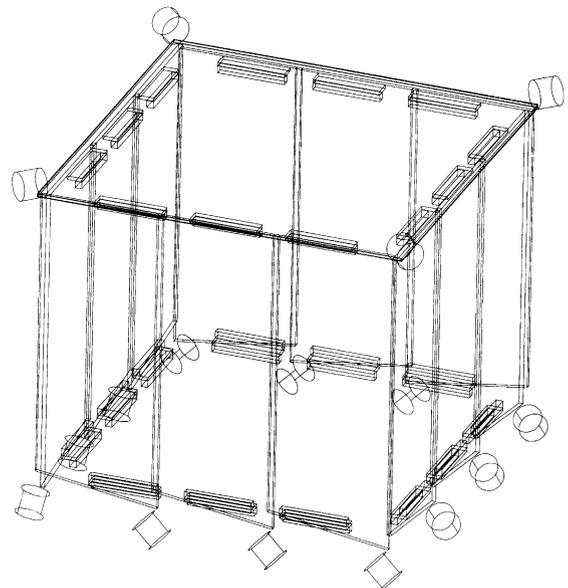

Fig. 3. Anticoincidence system. The overall dimensions are: length of 62.25 cm; width of 62.25 cm; height of 53.87 cm.
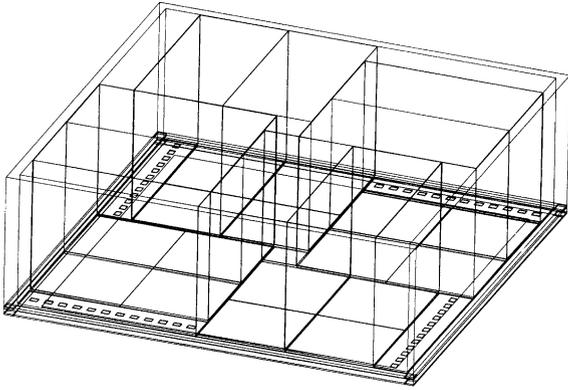
Fig. 4. Super-AGILE. Overall dimensions: length of 44 cm; width of 44 cm; height of 14.77 cm.

diffuse cosmic X-ray background. The distance between the gold mask and the top AC panel is 0.5 cm.

(6) *Thermal shield*: The thermal shield is modeled as an external Teflon layer (1 mm thick) plus an internal aluminum layer (10 μm thick). It covers the Mini-Calorimeter, the Tracker, Super-AGILE and the AC system.

(7) *Mechanical structure*: The description of the payload is completed by a preliminary model for the general support structure: four aluminum legs connected by other aluminum bars.

There is also a preliminary description of the Front-End Electronics (FEE) and of the trigger vertical boards, one for each lateral side of the payload, and one for the DH box, under the Mini-Calorimeter. They are described as some layers of silicon, ceramics and copper.

3.2. Silicon Tracker capacitive coupling, floating strip readout, and Gaussian noise

The electronic system for the AGILE Silicon Tracker is based on the "floating strip" readout. This implies that only one out of two contiguous Si-microstrips (each of 121 μm size) is read by dedicated electronic devices (TA1 chips). However, the capacitive coupling between contiguous strips allows not to loose any information. In the Monte Carlo code the capacitive coupling is simulated calculating the total energy release in every readout strip by the weighted sum as obtained in Ref. [7]. For the kth readout strip, the total energy release taking into account neighbour strips is $E_s(k) = E_i + 0.38\,(E_{i-1} + E_{i+1}) + 0.115\,(E_{i-2} + E_{i+2}) + 0.095\,(E_{i-3} + E_{i+3}) + 0.045\,(E_{i-4} + E_{i+4}) + 0.035\,(E_{i-5} + E_{i+5})$, where E_i is the energy release in the ith strip that can be either readout or floating, and $k = 1 + (i - 1) * 2$. This scheme for the capacitive coupling simulation is in agreement with test-beam results obtained from our group for a variety of incidence angles [6].

Instrumental noise was simulated as a Gaussian distribution with $\sigma = 5$ keV. We found that for a detection threshold of $\frac{1}{4}$ MIP $\simeq 27$ keV it has no macroscopic effects on the trigger rates. All the simulation results presented in this document have been obtained using the geometry model described above, taking into account the capacitive coupling and the floating strip readout, but without considering the noise that has negligible effects on the results.

4. Level-1 trigger

The Level-1 trigger for the Agile GRID is a hardware-implemented fast logic required to be very rapid (~ 2 μs), conceptually simple, easily implementable by a dedicated hardware, and using parameters reconfigurable by Telecommands. With Monte Carlo simulations we tested different trigger configurations, using the event classes (cosmic gamma-ray photons, background particles and Earth albedo-photons) described in Section 2. Here we present the main results.

Our best strategy for the Level-1 logic is based on the combined use of signals from AC panels and of the ratio R, defined as the ratio between the total number of fired TA1 and the total number of fired X and Y views: $R = $ (total no. of fired TA1)/ (total no. of fired X and Y views). In what follows, we call "R-trigger" the logic (implemented by a dedicated electronic component) regulating the use of both AC panels and R threshold values.

4.1. Level-1 trigger configurations

Here is a short description of the different Level-1 trigger configurations that we studied:

- PLA: events which give hits in at least 3 out of 4 consecutive planes (X OR Y view),
- TOP: PLA events which pass the TOP AC veto,
- LAT: TOP events with signals in 0 or 1 lateral AC panels, and TOP events which give signals in 2 consecutive AC panels or in 2 AC panels on the same side,
- LSI: LAT events with signals in 0 lateral AC panels, and LAT events with signals in 1 or 2 AC panels but with NO signal in the last silicon plane,
- R11G: LAT events with signals in 0 lateral AC panels, and LAT events with signals in 1 or 2 AC panels and $R > 1.1$.

PLA, TOP and LAT are consecutive steps, while LSI and R11G are the two final alternative trigger configurations. For comparison, in Tables 2–4 we reported also the number of events characterized by primary particles or photons reaching the tracker volume (TRA), a box of $38.06 \times 38.06 \times 21.078$ cm^3 which includes the tracker planes from the top sheet of the first tungsten layer to the bottom sheet of the last silicon-y plane.

In the case of gamma-ray photons it is important to observe that:

(1) gamma-photons giving a signal in the tracker may convert in the tracker volume, or in the Super-AGILE volume (mask or collimators). They can also convert elsewhere (mechanical structure, Mini-Calorimeter or bus MITA), or pass through the instrument without converting. We define as "good photons", those for which there is high probability to reconstruct the incident direction. By definition they are "tracker-converted photons";

(2) because of the presence of the Super-AGILE structure, some gamma-photons potentially able to enter into the Si-Tracker fiducial volume, because of their incidence angles and energies, can convert in the Super-AGILE structure. Their secondaries (electron and positron) may never arrive into the tracker volume. On the other hand, it can happen that some photons, that geometrically would not enter into the tracker volume, convert in the Super-AGILE structure, and their secondaries give a signal in the tracker then inducing a GRID background.

It is then useful to indicate with the suffix "TC" the photons converted in the tracker volume, and with the suffix "SC" the photons converted in the Super-AGILE structure. In the case of gamma-ray photons we also distinguish: (a) photons that theoretically, from a geometrical point of view, might enter into the tracker volume (TRA-TH),

Table 2
Level-1 trigger selection for background charged particles

	ELE (s^{-1}) (percent)	POS (s^{-1}) (percent)	HE PROT (s^{-1}) (percent)	LE PROT (s^{-1}) (percent)	TOTAL (s^{-1}) (percent)
TRA	787	688	123	147	1745
PLA	207	241	82	87	617
(% of TRA)	26	35	67	59	35
TOP	143	151	44	52	390
(% of TRA)	18	22	36	35	22
LAT	120	98	19	28	265
(% of TRA)	15	14	15	19	15
LSI	82	60	2	9	153
(% of TRA)	10	9	1	6	9
R11G	55	54	4	6	119
(% of TRA)	7	8	3	4	7

(b) primary photons actually entered in the tracker volume (PTRA), (c) primary photons converted in the tracker volume (PTCON).

4.2. Results and discussion

Tables 2–4 and Fig. 5 summarize our results in terms of alternative or progressive event selections. The TOP AC veto is useful to reject downgoing charged particles; the LAT AC veto discriminates events giving a signal either entering than exiting the detector (charged particles) from events which give signals only when they escape from the Tracker (photons into charged pairs). The R-trigger is a method optimized to reject non-interacting charged particles, based on a simplified idealization: when a non-interacting particle enters in the Tracker, only one track is expected; if the detector is crossed by a photon creating an electron–positron pair, two tracks are expected. Simulation results show that the R-trigger works very well with protons, and gives acceptable results also for electrons and positrons. In general, the method succeeds in discriminating photons from charged background particles very efficiently, sometimes better than the AC system. Clearly, the use of the R-trigger does not reject protons generating many secondaries or e^+/e^- producing

Table 3
Level-1 trigger selection for background albedo-photons

	ALB-1 PHOT (s^{-1})	ALB-2 PHOT (s^{-1})
TRA	748	1292
PLA	30	48
TOP	25	45
LAT	24	44
LSI	22	41
R11G	22	39

Table 4
Level-1 trigger selection for cosmic gamma-rays[a]

	PHOT HE 0-10 (event no.)	PHOT HE 50-60 (event no.)	PHOT LE 0-10 (event no.)	PHOT LE 50-60 (event no.)
TRA_TH	3144	3352	3144	3352
TRA	3511	3744	3433	3646
PTRA	2975	3054	3009	3175
PTCON	1488 (47%)	1292 (39%)	982 (31%)	892 (27%)
PLA	1683	1415	1171	908
PLA_TC	1434 (46%)	1102 (33%)	904 (29%)	694 (21%)
PLA_SC	168	128	95	44
TOP	1608	1355	1134	882
TOP_TC	1407 (45%)	1080 (32%)	895 (28%)	685 (20%)
TOP_SC	156	121	91	40
LAT	1578	1213	1129	872
LAT_TC	1383 (44%)	1006 (30%)	891 (28%)	681 (20%)
LAT_SC	150	102	90	40
LSI	1243	829	1071	833
LSI_TC	1117 (36%)	690 (20%)	844 (27%)	652 (19%)
LSI_SC	94	77	89	40
R11G	1469	1029	998	766
R11G_TC	1258 (40%)	858 (26%)	803 (26%)	606 (18%)
R11G_SC	136	84	72	36

[a] In parenthesis we reported the percentage of selected events respect to the total number of photons that theoretically could enter into the tracker volume (% of TRA_TH).
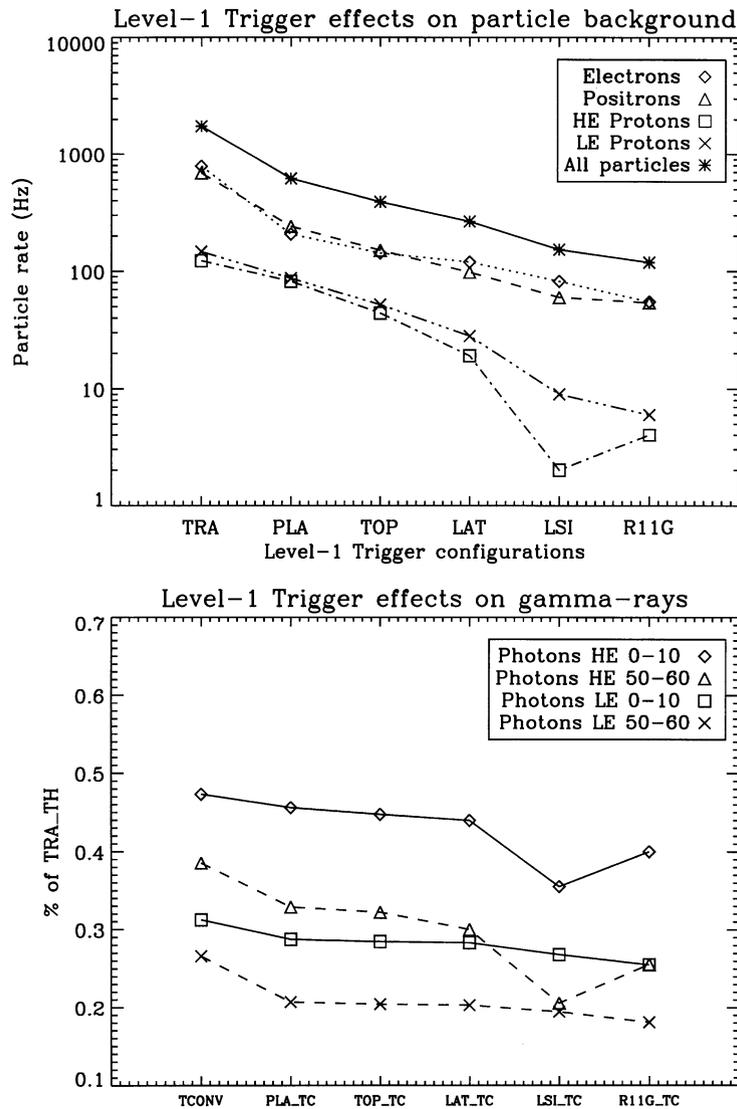
Fig. 5. Particle background rates for different Level-1 trigger configurations and Level-1 trigger efficiency for different photon classes. Event selection based on TRA, PLA, TOP and LAT are sequentially applied to all events. Further selections based on LSI or R11G are instead mutually exclusive. The suffix "TC" denotes "Tracker-converted".

secondaries and electromagnetic showers. A trigger configuration based only on the AC system does not reject low energy protons stopping inside the tracker. The two methods are based on different "philosophies" and they both give good results in different situations.

From our simulations it appears that the best choice is a combination of the two strategies and that the most efficient Level-1 trigger configura-tion is R11G, rejecting ~93% of background particles without affecting significantly the gamma-ray detection rate.

5. Level-1.5 data processing

The additional "Level-1.5" data processing uses the tracker discretization in terms of TA1 chips

$(3.1 \times 3.1 \text{ cm}^2$ square elements), together with the complete AC and MC information. We investigated the efficiency of alternative Level-1.5 Trigger options in rejecting background charged particles and here we present the main results.

5.1. Level 1.5 trigger configurations

We considered the following options:

- DIS: The DIS option is a simplified track reconstruction and is based on computing the distance D of the fired TA1s from the fired AC lateral panel. The basic idea is that a charged particle is expected to have increasing D values as a function of increasing plane, while a gamma-ray photon is expected to have a decreasing D function (in the restricting hypothesis that they both come downward and in the absence of strong "hard" scattering of photon-created pairs). The parameter DIS is defined as: $\text{DIS} = D_{\text{fp}} - D_{\text{lp}}$ where D_{fp} is the distance of the closest fired TA1 to the fired AC lateral panel in the first plane, while D_{lp} is the distance of the closest fired TA1 to the fired AC lateral panel in the last plane. We require $\text{DIS} \geqslant 0$ for good events. This option is applied only if there are fired AC lateral panels.
- RUD10 (or RUD12): The fired tracker views are divided in two groups (UP and DOWN) and the ratio R is computed separately for the two groups (R^{up} and R^{down}). The ratio $\text{RUD} = R^{\text{up}}/R^{\text{down}}$ can help in discriminating good gamma-photons, that come downward, from secondary photons generated by charged particles, that come from the bottom toward the top

of the detector. With the option RUD10 are rejected all the events with $\text{RUD} > 1.0$, while with the option RUD12 are rejected all the events with $\text{RUD} > 1.2$.

- VFORM: This option, as RUD10 and RUD12, can help in discriminating primary photons going downward from secondary photons coming upward. It computes the separation S between fired TA1 on the same view, divides the fired planes in two groups (UP and DOWN) and compares the mean separation of the UP planes with the mean separation of the DOWN planes. The parameter V is defined as $V = S_{\text{down}} - S_{\text{up}}$ and events with $V < 0$ are rejected.
- CGAP: This option rejects events with a gap of more than 2 planes (4 views) between the MC and the last fired tracker view. It is applied only if there is a signal from the MC and it is supposed to reject events due to e^+ or e^- which stop in the MC and generate a secondary photon which enters the tracker upward and creates a couple only after passing 4 or more views.
- TGAP: This option rejects events with a gap of more than 2 planes (4 views) in the tracker. The parameter T_GAP is defined, for a single event, as the maximum number of no-fired views between two non-consecutive fired views.

5.2. Results and discussion on the Level-1.5 trigger processing

Tables 5 and 6 and Fig. 6 show the simulation results. The simple DIS algorithm is the most efficient in rejecting background particles without

Table 5
Summary of Level-1.5 processing of background events

Type	R11G (s^{-1})	DIS (s^{-1})	RUD12 (s^{-1})	RUD10 (s^{-1})	VFORM (s^{-1})	CGAP (s^{-1})	TGAP (s^{-1})
ELE	55	35	41	36	45	52	46
POS	54	30	43	36	42	50	43
LE PR.	6.2	3.4	4.9	4.2	5.8	5.8	5.8
HE PR.	4.1	1.5	2.8	3.1	3.2	4.0	3.8
Total	119	70	92	79	96	112	99
ALB-1	22	20	17	18	19	21	18
ALB-2	39	36	30	33	35	36	33

Table 6
Summary of Level-1.5 processing of cosmic gamma-ray events[a]

Photon class	R11G (TC) (%)	DIS (TC) (%)	RUD12 (TC) (%)	RUD10 (TC) (%)	VFORM (TC) (%)	CGAP (TC) (%)	TGAP (TC) (%)
HE 0–10	40	39	39	36	35	39	38
HE 50–60	26	25	24	21	19	26	23
LE 0–10	26	26	23	20	25	22	24
LE 50–60	18	17	14	12	15	16	15

[a] Simulation results concerning only Tracker-Converted (TC) photons. Values in the table represent the percentage of the number of simulated events that pass the different Level-1.5 trigger options respect to the total number of photons that theoretically could enter into the Tracker volume (% of TRA_TH).
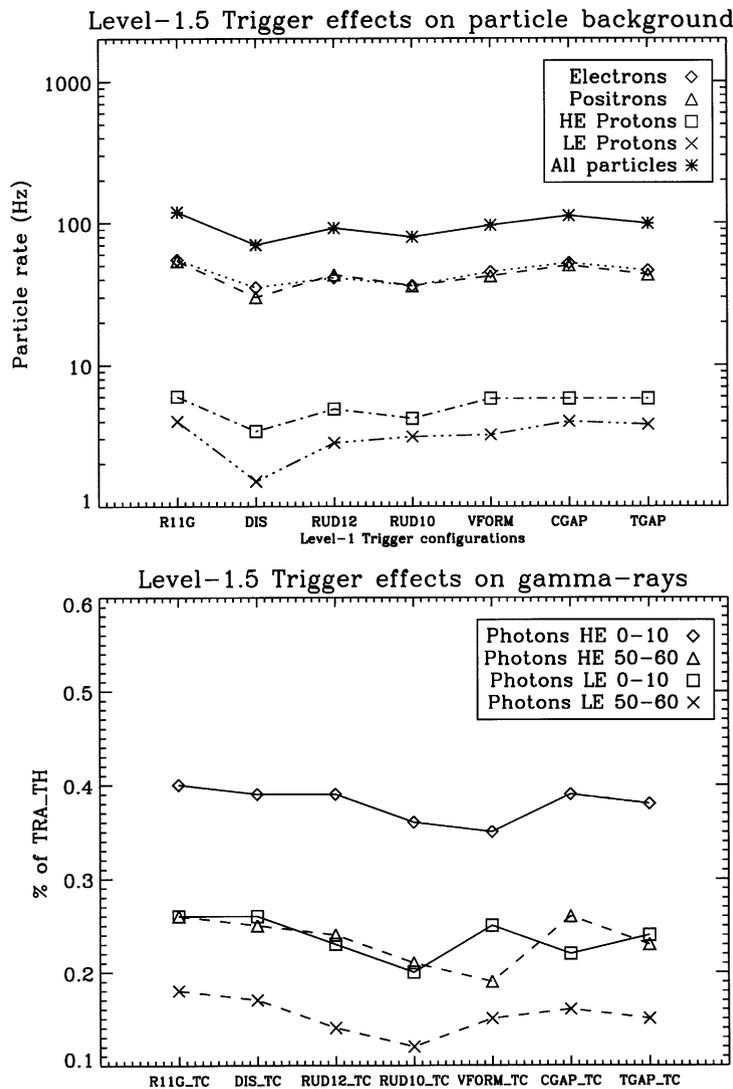

Fig. 6. These plots show the efficiency of the Level-1.5 trigger alternative options in rejecting particle background and in detecting gamma-photons (DISRUD means (DIS+RUD_10) and DISCG means (DIS + C_GAP)).

losing too many good photons. This algorithm is applied only if there is at least one fired AC lateral panel; most of background charged particles verify this condition, while good photons often do not hit any lateral AC panel.

Options RUD10, RUD12 and VFORM are not very efficient because the distributions of the RUD and V parameters are not significantly different for background particles and for good photons. The C_GAP option is not efficient because the majority of background electrons, positrons and albedo protons do not give a signal in the Mini-Calorimeter. There are no significant differences between the background particle T_GAP distributions and the photon T_GAP distribution, probably because this parameter is influenced by secondary particles.

6. Discussion and conclusions

By using a complete and detailed model of the AGILE instrument, we simulated with GEANT the performance of the on-board Level-1 trigger logic. We obtain satisfactory results from our optimization study of the Level-1 and 1.5 trigger logic for the cosmic gamma-ray signal (with photon energies between ~ 30 MeV and 50 GeV) and for the rejection of the particle and albedo-photon backgrounds in a 550 km equatorial orbit. The optimal Level-1 (and therefore necessarily simple) event selection algorithms are the R11G and DIS procedures that can be easily hardware-implemented and are very fast ($\leqslant 20$ μs). Table 7

summarizes the main results of our paper: the total background rates expected for two different Earth occultation geometries. At the Level-1 + 1.5 the background component completely dominates the event rate over the cosmic gamma-rays by a factor between 10 and 100, and the total background event rate is near 100 s^{-1}, a value which can be sustained by the on-board AGILE Data Handling [2]. Therefore the Level-1 logic presented here is adequate for the AGILE GRID.

We also note that the albedo-photons contribute a significant fraction (between $\sim 30\%$ and more than $\sim 50\%$ depending on the Earth's position with respect to the GRID) of the total background rate. Since these photons are dominated by 10–100 MeV gamma-rays, Level-1 techniques are not adequate in substantially reducing their event rate, and a special Level-2 data processing is required, which will be the subject of a forthcoming paper.

Our results are of general interest for space detectors similar to the AGILE GRID. Two conclusions are of particular interest: (1) the fact that low-energy leptons (magnetospheric trapped electrons and positrons) dominate the particle background requires special attention and a proper event selection logic; (2) Earth albedo-photons constitute a substantial fraction of the residual events passing the Level-1 trigger stage.

Table 7
Average GRID Background Event Rates after Level-1+1.5 Processing

Background component	Unocculted GRID FOV (s^{-1})	Half-occulted GRID FOV (s^{-1})
Charged particles	70	70
Earth albedo-photons	20	40
Total	90	110

References

[1] M. Tavani, et al., (2002) in preparation.

[2] M. Tavani, et al., Invited paper presented at the Gamma 2001 Symposium, Baltimore, 4–6 April 2001, American Institute of Physics Conference Proceedings, 587 (2001) 729.

[3] M. Tavani, et al., Science with AGILE, AGILE Internal Note, A-P-019, 2001, (http://www.ifctr.mi.cnr.it/Agile).

[4] V. Cocco, F. Longo, M. Tavani, Nucl. Instr. and Meth. A 486 (2002) 623.

[5] R. Brun, et al., GEANT Detector Description and Simulation Tool, 1993, CERN, Geneva.

[6] G. Barbiellini, et al., INFN/TC01/006, Nucl. Instr. and Meth. A (2002) submitted for publication.

[7] G. Fedel, Dissertation for the Laurea in Physics, University of Trieste, 2000.

[8] M. Prest, et al., (2002) in preparation.

[9] C.E. Fichtel, et al., Astrophys. J. 198 (1975) 163.

[10] D. Thompson, 1999, private communication.

[11] M. Feroci, et al., In-flight performances of the BeppoSAX gamma-ray burst monitor, in: Proceedings of the SPIE Conference, 1997, Vol. 3114, San Diego.

[12] R. Battiston, Search for antimatter in space with the Alpha Magnetic Spectrometer, `astro-ph/9907152`, Presented at 13th Les Rencontres de Physique de la Vallee d'Aoste: "Results and Perspectives in Particle Physics", 1999.

[13] J. Alcaraz, et al., Phys. Lett. B 472 (2000) 215.

[14] J. Alcaraz, et al., Phys. Lett. B 484 (2000) 10.

[15] S.V. Koldashov, et al., Electron and positron albedo spectra with energy more than 10 MeV, Proceedings of the 24th ICRC, 1995, Vol. 4, p. 993.

[16] V. Cocco, P. Lipari, F. Longo, Note on the charged particle albedo fluxes, AGILE Technical Note, AGILE-SIM-TN-002, 2000.

[17] D.J. Thompson, G.A. Simpson, M.E. Ozel, J. Geophys. Res. 86 (1981) 1265.

[18] E. Costa, E. Massaro, M. Salvati, A. Apolloni, Astrophys. Space Sci. 100 (1984) 165.

[19] J.C. Ling, Ph.D. Thesis, 1974, UCSD.

[20] J.L Matteson, J.C. Ling, L.E. Peterson, Proceedings of the Ninth ESLAB Symposium, 1974, p. 137.

[21] V. Schoenfelder, U. Graser, J. Daugherty, Astrophys. J. 217 (1977) 306.

[22] V. Schoenfelder, F. Grami, F.P. Penningsfeld, Astrophys. J. 240 (1980) 350.